

Received July 13, 2020, accepted July 29, 2020, date of publication August 4, 2020, date of current version August 17, 2020.

Digital Object Identifier 10.1109/ACCESS.2020.3014139

Real-Time AR Technology Assisted High-Resolution Image Processing and Its Graphic Design Application

TING SHENG 

Academy of Art and Design, Wuchang University of Technology, Wuhan 430223, China


e-mail: shengting180627@163.com

ABSTRACT Based on real-time AR technology, this article processes high-resolution graphics and uses it in graphic design. A high-resolution image equalization algorithm based on the maximum entropy model is proposed. First, use the Otsu method to determine the data segmentation point of high-resolution graphics; then preprocess the high-resolution image; then traverse according to the proposed maximum entropy model to find the dynamic range segmentation point that maximizes the image entropy after equalization, and finally according to the data segmentation point and dynamics, the range division point performs high-resolution image equalization on the image to obtain the final enhancement result. Experiments show that compared with other comparison algorithms, the algorithm has a wide application range, strong detail retention ability, and natural effect. Experiments show that compared with other contrast algorithms, this algorithm has a proper contrast improvement, a wide range of applications, can be used for real-time video enhancement and graphic design and is practical. In the graphic design stage, the involvement of digital technology has become a basis for designers to choose horizontal solutions. In the early stage site design and mid-term graphics selection, the performance analysis software in BIM was used to analyze the acousto-optic heat of the plane. Based on this intuitive data analysis, the scheme was weighed. At the same time, the VR three-dimensional space experience reinforces the “people-oriented” design principle. With the help of digital technology, the designer compares the solutions horizontally from the perspective of rationality and sensibility, to choose the sustainable design of graphic design.

INDEX TERMS Real-time AR technology, high-resolution images, graphic processing, graphic design.

I. INTRODUCTION

The medium of human transmission of information in daily life is mainly language and images, and scientific research and statistics show that about 75% of the information that humans obtain from the outside world comes from the visual system, which is obtained from images [1]. This shows that image information plays a very important role in the transmission of information [2]. The images collected by the early image acquisition equipment are all analog quantities. Such images are called analog images, which can be described by a continuous function, which is characterized by the continuous change of the position of the light and the intensity of the light [3]. The processing speed of the analog image is fast, but its accuracy is low and its flexibility is poor. It has no judgment function and non-linear processing function, which is not conducive to processing by the computer,

The associate editor coordinating the review of this manuscript and approving it for publication was Zhihan Lv .

and it is not convenient for transmission and storage [4]. Later, with the development of technology, computers gradually became popular, and people began to use computers to process images [5]. However, due to the characteristics of computers, it cannot directly process analog quantities. Therefore, we need to discrete the amplitude and position of continuous analog images [6]. Finally, a digital image is formed and then processed by a computer. The transmission speed of digital images is fast, the versatility of storage is strong, the precision is high, and the processing method is flexible. Due to these characteristics of digital images, it has become the main research object of image processing. Image enhancement is an important branch in the field of digital image processing [7]. It is an image processing technology that processes low-quality images to make them clearer and more beautiful and improve their quality [8]. In many cases, the poor final image quality is limited by the conditions of the scene. At this time, to improve the visual effect of the image, we will use image enhancement technology [9]. For example,

we can highlight some characteristics of the target object in the image or extract the characteristic parameters of the target object, etc [10]. These operations are conducive to our recognition, tracking, and understanding of the target in the image. The main content of image enhancement processing is to highlight the parts of interest in the image and weaken or eliminate the content that we do not care about or need. In this way, useful information can be strengthened, so that the image becomes more practical or more suitable for us or the machine to analyze and process. Research on fast and effective image enhancement algorithms is one of the key contents to promote the development of image analysis and image understanding [11].

Alarcon first proposed Brightness preserving bi-histogram equalization (BBHE), which divides the input high-resolution graphics into two sub-high-resolution graphics based on the average brightness of the image, and then equalizes the two sub-high-resolution graphics [12]. Various improved algorithms of BBHE appeared in the follow-up: there are median-based segmentation points, such as dualistic sub-image histogram equalization (DSIHE) proposed by Malmström *et al.* [13]. There are based split points, such as threshold and optimized histogram equalization proposed by Liem and de Reijke [14]; there are also based on the average, but after adjusting the sub-high resolution graphics and then equalizing, such as Ishafit *et al.* proposed brightness preserving and contrast limited bi-histogram equalization and brightness preserving and non-parametric modified bi-histogram equalization [15]. The above types of algorithms all have corresponding recursive or iterative forms, such as recursive mean-separate histogram equalization (RMSHE) proposed by Wang and minimum mean brightness error Bi-Histogram equalization (MMBEBHE) proposed by Wang *et al.* [16]. They are all based on the iterative form of image mean; and recursive sub-image histogram equalization (RSIHE) proposed by Pouladzadeh is an iterative form based on image median [17]. The disadvantages of these brightness-maintaining algorithms are not suitable for low-illumination and high-brightness images, because their brightness-maintaining characteristics are advantages for normal brightness images, but for low-illumination and high-brightness images, brightness maintenance is disadvantageous [18]. Yes, this also limits the application range of brightness-preserving algorithms [19]. Ji P *et al.* proposed weighted threshold histogram equalization (WTHE), which transforms high-resolution graphics with a mapping function before the equalization operation, and uses this mapping function to enhance small data and suppress spikes [20]. This solution to a certain extent improves the problem of excessive enhancement of traditional high-resolution graphic equalization and loss of details, but the fixed parameters result in poor results for some images [21]. Doshi and others proposed weighted histogram equalization (WHE), which adds weight to the data of each gray level on the high-resolution graphics to adjust the high-resolution graphics and then equalizes the adjusted high-resolution graphics change [22]. This scheme

can reduce the stretching degree of high-resolution graphics and avoid excessive enhancement, but the parameters are also fixed values, and small data and large data in high-resolution graphics are processed uniformly without distinction, which results in its processing results for many images [23].

In the digital age, mobile internet advertising has attracted the attention of businesses and consumers as an advertising form that can directly hit the audience's psychology [24]–[26]. Commercial advertising design is no longer confined to the two-dimensional plane world. Advertising designers can make full use of the advantages of wireless terminals, and use AR, VR, and other technologies in the emerging technology field to make commercial advertising more interactive and interesting. Instead of blindly duck-feeding output to consumers, this will backfire, causing consumers to resist and even ignore the content of the advertisement. Excellent Internet commercial advertising design should not only seize the sales opportunity to make the merchant products stand out from many homogeneous products, but also keep the novel and unique in content, break through the traditional static expression of commercial advertising in design, and aesthetically keep up with the time's pace. Such commercial advertisements can stimulate consumers' desire to buy and become the "golden key" to achieve purchases, and at the same time increase the popularity and sales of products. This article analyzes the shortcomings and causes of the existing improved high-resolution graphic equalization algorithm, and based on this, a dual high-resolution graphic equalization algorithm based on the maximum entropy model is proposed, and then further optimization based on the algorithm is proposed. A global high-resolution graphic equalization algorithm based on a hybrid model is presented. The main contributions of this article are important, it studies graphic design through an improved high-resolution graphics processing algorithm, and uses a real-time AR technology system to conduct in-depth discussions, introduces the theoretical basis of high-resolution graphics equalization and some image quality evaluation indicators, and divides the current improved algorithms into two categories.

II. REAL-TIME AR TECHNOLOGY-ASSISTED HIGH-RESOLUTION GRAPHICS PROCESSING DESIGN

A. IMPROVED HIGH-RESOLUTION GRAPHICS PROCESSING ALGORITHM

High-resolution graphic equalization is a commonly used technology in image enhancement. Its main idea is to change the gray-scale high-resolution graphics of the input image into a uniform distribution in the entire gray range, thereby pulling adjacent gray levels apart and improving the image [27]. Count the number of pixels in each gray level of the input image.

$$D(i) = \frac{h(i)}{N}, \quad i \in [0, M - 1] \quad (1)$$

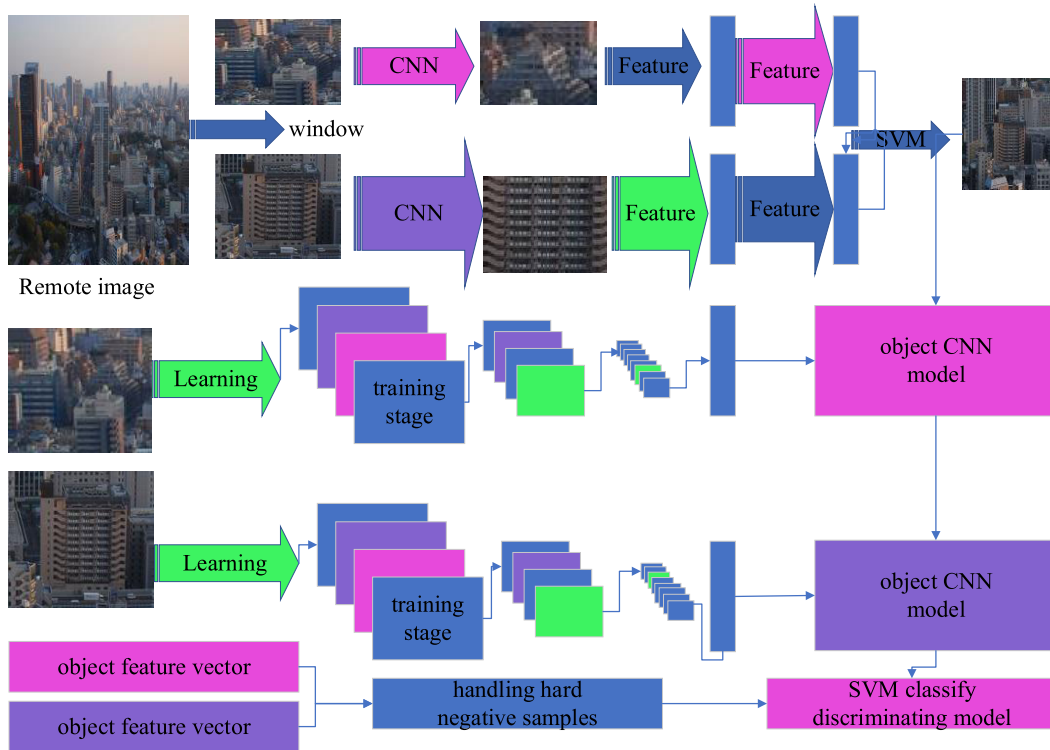


FIGURE 1. Improved high-resolution graphics processing algorithm.

Calculate the cumulative distribution high-resolution graphic D of the input image by the gray-scale distribution probability high-resolution graphic $cdf(i)$, namely:

$$cdf(i) = \sum_{n=1}^i D(n), \quad i \in [0, M - 1] \quad (2)$$

Multiply the cumulative distribution high-resolution graphic $cdf(i)$ by the total gray range to obtain the mapping table. In formula (2), use round to indicate rounding and rounding, that is:

$$tab(i) = r((M - 1) \times cdf(i)), \quad i \in [0, M - 1] \quad (3)$$

The high-resolution graphic equalization effect and high-resolution graphic changes are shown in Figure 1. It can be seen from the figure that high-resolution graphic equalization stretches the grayscale with a relatively concentrated distribution into the entire grayscale range, making the gap between the grayscales larger, thereby improving the contrast of the entire image; but at the same time, it also merges some gray scales are caused, which causes some details to be lost [28]. This can be verified from the blurring of the riverbed part and the saplings in the river after the equalization.

The main principle is to divide the high-resolution graphics of the input image into left and right sub-high-resolution graphics using mean, and then perform high-resolution graphic equalization on the two sub-high resolution graphics respectively [6]. Because it is based on the image mean segmentation, the equalized image mean value will

not deviate too much from the original image mean value, to achieve the purpose of maintaining brightness, calculate the input image mean G_{mean} , according to the mean G_{mean} will divide the original high-resolution graphics into two high-resolution graphics. Calculate the gray distribution probability high-resolution graphics D_M and D_R of the left and right sub-high-resolution graphics separately, namely:

$$D_M(i) = \frac{h(i)}{N_M}, \quad i \in [0, M - 1] \quad (4)$$

$$D_R(i) = \frac{h(i)}{N_R}, \quad i \in [0, M - 1] \quad (5)$$

Among them, N_M and N_R represent the total number of pixels of the left and right sub-high-resolution graphics, and M represents the total gray level of the image [29].

Calculate the cumulative distribution of high-resolution graphics D and G of the left and right sub-resolution graphics, namely:

$$cdf_M(i) = \sum_{n=1}^i D_M(n), \quad i \in [0, G_{mean}] \quad (6)$$

$$cdf_R(i) = \sum_{n=G_{mean}}^i D_R(n), \quad i \in [0, G_{mean}] \quad (7)$$

Calculate the left and right two mapping tables $tab_{G_{mean}}$ and $tab_M(i)$, and merge to get the final mapping table tab , where round means rounding, ie:

$$tab_M(i) = r((G_{mean} - 1) \times cdf_M(i)), \quad i \in [0, G_{mean}] \quad (8)$$

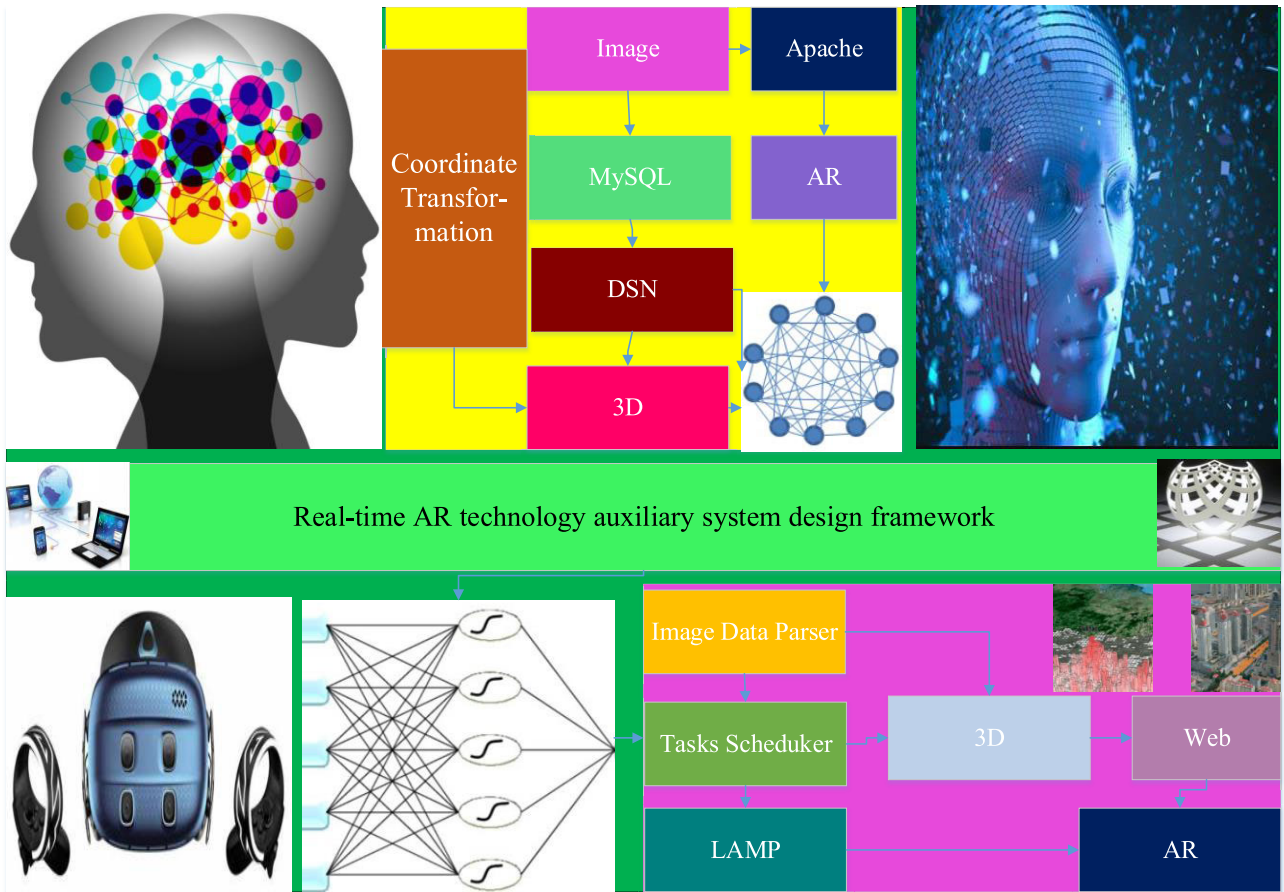


FIGURE 3. Real-time AR technology auxiliary system design framework.

method [32], [33]. It is a linear equation solution method based on Krylova subspace. The pre-optimal conjugate gradient method first preprocesses the matrix G to make its eigenvalue distribution concentrated, thereby speeding up its convergence speed, and the conjugate gradient method has been proved theoretically to converge through a finite number of iterations. The computational cost of the conjugate gradient method is mainly the product of matrix A and vector. When matrix G is sparse, the amount of calculation can be greatly reduced.

B. DESIGN AND ANALYSIS OF REAL-TIME AR TECHNOLOGY AUXILIARY SYSTEM

The requirements of the video call client for real-time communication are expanded, and the relevant factors that the client needs to pay attention to during the design process are also elaborated. The main purpose of this product has the following two points. The first point is to require the client to be used normally in low-light environments, and the second point is that the client must be able to adapt to the existing AR server [34]. The low-illumination video quality enhancement algorithm is implemented based on the dark primary color prior principle, and the video denoising is implemented by improved fast guided filtering. The module

adapted to the existing AR server is implemented by the AR application-layer client gateway. The main body of the client depends on the AR technology, and the algorithm and the gateway can be applied to the client in a certain way. Research and application of a low-illumination video quality enhancement technology to improve the video quality under low-light conditions and reduce noise. This article proposes a low-illumination video quality improvement algorithm based on dark primary color prior, which reduces the noise generated by the algorithm through fast guided filtering, and the processing speed is extremely fast, which can meet real-time performance. By combining this technology with WebRTC technology, the algorithm is applied to the WebRTC client, which not only can meet the interworking of multiple types of terminals, but also enhances the adaptability of the terminal in dark light environments. This client is based on the WebRTC project, equipped with a low-illumination enhancement algorithm, and takes into account the SIP protocol through the conversion of the gateway. From the results, it can be seen that the client can effectively complete the connection with the SIP protocol terminal in practical applications, and It has good adaptability in dark light environment, improves the user’s subjective experience, and improves the video quality of real-time communication, as shown in Figure 3.

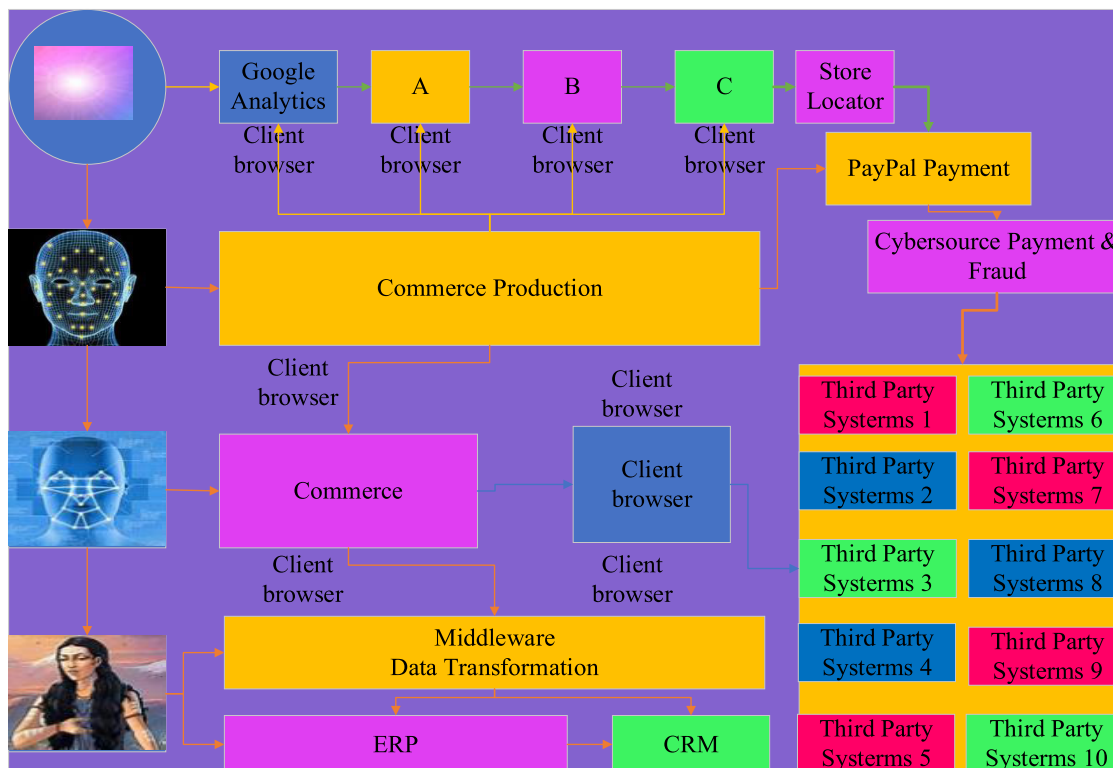


FIGURE 4. High-resolution graphics edge information processing.

The core part of the real-time communication video quality enhancement client designed in this article is the low illumination video quality enhancement algorithm. In the past, low-illumination image quality enhancement algorithms were rarely used in real-time video communication. There are two biggest reasons [4]. One is that due to the limitations of night photography, more noise will be generated, and the noise will be amplified after the brightening process, resulting in more images in the final image. The second is that due to the complex operation of the brightening process and a large amount of image matrix calculation, it is difficult to ensure real-time performance. The low-illumination video lifting algorithm designed in this article has faster speed and can meet the requirements of real-time video. Therefore, the use of this algorithm in this client is feasible. At the bottom layer are various interfaces provided by the platforms to the terminal. This type of interface enables the terminal to control the hardware and complete the functions below the transport layer. The top-level UI only needs to know the interface provided by the business logic and provide corresponding functions to the user. From the perspective of the architecture of the real-time communication-oriented video quality enhancement client, the focus of this article is on the design of low-illumination video quality algorithms and the conversion design of SIP signaling and WebRTC signaling. Finally, this article also needs to focus on the content, that is, the application of low-light video quality enhancement algorithms on the WebRTC client.

When dealing with this problem, there are many solutions, such as preprocessing dark images, first reducing noise in a certain way, and then brightening the image after noise reduction, this can make the processed image reduce a lot of noise. But this also causes two problems. One is that the processing time is too long. In general, it takes about 0.75s to perform noise reduction on a 1920*1080 resolution image, and then use a general brightening algorithm, such as LIME or Retinex algorithm. This time may seem short, but it cannot meet the requirements in real-time communication. 15 frames are the minimum for real-time communication. When the frame rate of the video is lower than 15, the human eye cannot form a continuous image in the brain. For 15 frames, the processing speed of a single image is less than 0.075 seconds. Therefore, there are few ways to improve low-light video through software, basically through hardware. Second, when noise reduction is performed on the image, it also smooths out some edge information of the image. The biggest difference between noise and edges is that the pixel gradient around the nose area is generally large, and centered on the noise, the change in the surrounding gradient is similar. The edge has a gradient step, and in the normal direction of the edge of the image object, the sudden change of the pixel gradient can be clearly discerned, and the pixel gradient gradually decreases from the normal direction to the tangent direction of the edge. General filtering cannot distinguish between noise and edges, so the edge information can only be processed in the way of dealing with noise, which causes the edges to be blurred, as shown in Figure 4.

According to the overall WebRTC framework, if you need to optimize the video on the server-side, you need to configure an additional streaming server. The media streaming server needs to be configured with the six modules described above. The workflow of the media streaming server is as follows: the business logic server uses a built-in listener to detect whether the client sends data. After detecting the data sending request, if the forwarding request from the WebRTC server is received at the same time, the corresponding audio and video data will be stored in the buffer through the transceiver module. Next, the audio and video codec module encodes and decodes the data stream, the media stream processing module optimizes the video call enhancement algorithm, and then the media stream synchronization module performs audio and video synchronization operations, and finally forwards the complete media stream processed by the media server give each client to realize the enhanced video call function.

After analyzing the previous two high-resolution graphic equalization algorithms, it is found that they still have some problems. For the dual high-resolution graphic equalization algorithms of brightness maintenance, brightness maintenance is not only their advantage but also the reason for their limited application range. They can have the characteristic of maintaining brightness because they divide the high-resolution graphics according to certain characteristics of the image so that the brightness change after the final equalization is not much different. However, for low-illumination and high-brightness images, maintaining the brightness will result in poor results in the final image. Therefore, to expand the application range of the dual high-resolution graphic equalization algorithm, dual-high resolution graphic equalization algorithms with variable brightness have been proposed one after another. Their main idea is to select the split point of the high-resolution graphics data and the dynamic range split point separately, so that the data of the left and right sub-high-resolution graphics can be balanced within a suitable range. However, the selection scheme of the dynamic range segmentation point is mostly relatively simple, and the optimal value is not selected under a certain measure. The difference between the dual high-resolution graphic equalization algorithm based on the maximum entropy model and other variable brightness dual high-resolution graphic equalization algorithms is that it is an optimization process for the selection of the dynamic range segmentation point, so the final dynamic range segmentation point is obtained. It is an optimal solution under the maximum entropy model.

III. AR TECHNOLOGY-ASSISTED GRAPHIC DESIGN APPLICATION DESIGN

A. ANALYSIS OF GRAPHIC DESIGN METHODS

The traditional visual experience is relatively stable compared to the work, and the graphic design in the modern background has required to present a visual three-dimensional form, making the visual form more prominent and the visual

tension more intense, to achieve the purpose of attracting the viewer's eye. To achieve this goal, we need to carry out innovative experimental exploration from the form of composition, breaking the old visual balance to create an unconventional visual experience. Vision is the feedback after the image of the retina is transmitted to the brain. An optical illusion is a form of expression in the construction of three-dimensional space. The application of the law of optical illusion can enable our design works to create a multi-dimensional mixed space by combining different dimensions. It has become a new design method. This kind of visual effect can show three-dimensional authenticity, and beyond the traditional thinking and visual habits, you can enjoy "visual deception" to achieve the fundamental purpose of the design. The use of this artistic technique can recreate objective objects, subvert the traditional spatial-visual logic, create a new visual focus of the work, and construct a three-dimensional space in a novel way. This visual form has a strong expressive force. Create new visual effects using common faces, alternating, and juxtaposition, as shown in Figure 5.

Graphic design is mainly to express the ideological connotation of the work and enhance the transmission of information, but to reflect the richness of the work. In addition to the design methods such as the innovation of visual elements, the use of creative ideas, the three-dimensional composition of dots, lines, and planes, the visual impact of color contrast. It is also one of the main factors for enriching design creation. The use of color can enhance the sense of space, make the design elements tend to three-dimensional space, and enhance the visual aesthetics of the graphic design. Color is a very effective expression tool for three-dimensional space, as a visual element has its unique artistic expression in the expression of the picture. Color is also a feeling of the human visual nerve. It is inseparable from the space environment, object shape, light and shadow, and our eyes. Color has variability in the structure, space, quantity, and quality of performance, which makes the graphic elements produce virtual and real contrasts. Human vision has the function of accepting the color of the entire spectrum, so staring at a color for a long time will affect the color perception nerves. From the hue of the color, warm tones give a visual sense of closeness compared to cool tones, and cool colors have a sense of distance; and cool colors seem to shrink, while warm colors look inflated. The visual color contrast of the works gives viewers the illusion of near and far and deep and light illusions, creating a three-dimensional sense of space visually.

The purity comparison is divided into the hue purity comparison of the same color system, and the comparison between the same purity of different color systems. In the comparison of the purity of the same color system, placing color with the same purity in the same color system with lower purity will distinguish it, and placing two colors in the same color system with higher purity will merge. The different color purity of the visual picture will convey different

TABLE 1. Comparison of SWSS and fat-tree connection characteristics.

Sequence	ASPL(ms)	RWA (mm)	SWSS (kHz)
Axial position T1WI	4417	605	2554
Oblique axis position T2WI	5745	645	4154
Coronal T2WT	5747	514	7154
Sagittal T2WI	5757	284	4047
Axial T2WI fat compression	5752	254	2974
Axial DWI	4725	752	5212
Axial position LAVA	8142	67	8014

algorithm is also optimized and accelerated. OpenMP is used to enable multi-thread acceleration to further accelerate the processing speed, and finally realize real-time processing of 1080p video. Next, these two acceleration processes will be described in detail. The multithreading of the system software is mainly reflected in that the acquisition process and the enhancement process are carried out by one thread, but because the data must be processed during the acquisition and enhancement, this involves data competition. To avoid this problem, it is necessary to ensure that after the acquisition is completed, the enhancement operation has been completed when the data is filled, and when the enhancement operation is performed, it must be ensured that a frame of data has been filled. Therefore, two notification events need to be registered to identify the filling process and the state of the enhanced process, so that multi-threaded acceleration can proceed smoothly. The logical block diagram of this process is shown in Figure 6.

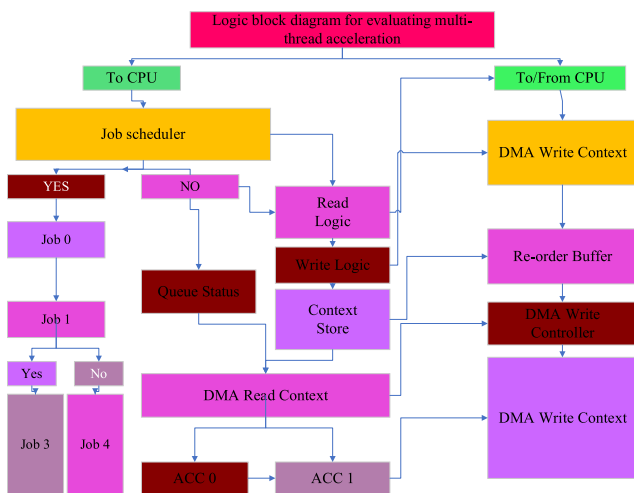


FIGURE 6. Logic block diagram for evaluating multi-thread acceleration.

On the left is the thread for video capture, and on the right is the thread for video enhancement. The sign of filling completion is that the filling completion event becomes a signal, and the sign of enhancement completion is that the

enhancement completion event becomes a signal. After they become signaled, the thread will continue, and the corresponding notification event will be set to no signal state; before this, the thread will have been waiting in this part, so that the problem of data competition will not occur to ensure that the two threads execute correctly.

OpenMP abstractly describes the parallel algorithm, so that the programmer only needs to add a dedicated pragma to the source code, the compiler will automatically parallelize the following code, and the synchronization mutual exclusion and communication functions it provides can effectively avoid data competition. When we comment out these pragmas, or the compiler does not support OpenMP, the program will automatically degenerate into a normal serial execution program without manual modification.

Since OpenMP describes parallelism at a high-level abstraction, this reduces the difficulty and complexity of parallel programming, which saves a lot of programmer energy and allows us to focus on the algorithm rather than the specific implementation details of its parallel processing. OpenMP is suitable for multi-threaded programming based on data diversity and provides greater flexibility because it can be easily adapted to configurations in different parallel systems. OpenMP takes over the work of thread granularity and load balancing, both of which are problems in traditional multi-threaded programming. However, if synchronization and mutual exclusion between threads are more complicated, OpenMP is not very applicable.

IV. RESULTS ANALYSIS

A. ANALYSIS OF HIGH-RESOLUTION GRAPHICS PROCESSING RESULTS

To verify the enhancement effect of the dual high-resolution graphic equalization algorithm based on the maximum entropy model, we selected multiple public image databases for testing. We selected BBHE, BPCLBHE, ESIHE, and DRSHE as comparison algorithms, where BBHE is the classic brightness maintenance double high-resolution graphic equalization algorithm, BPCLBHE is a brightness-preserving double high-resolution graphic equalization algorithm in recent years. ESIHE although the high-resolution graphic data division point is consistent with the dynamic range division point, it is a variable-luminance double-high resolution graphic equalization Algorithm, the final DRSHE is a high-resolution graphic dual-resolution graphic equalization algorithm where the high-resolution graphic data segmentation point and the dynamic range segmentation point are inconsistent. We will compare and analyze the enhancement effect of our algorithm and other comparison algorithms from the subjective and objective aspects. The subjective analysis mainly depends on people’s judgment, which is related to personal visual experience. Therefore, to get a relatively fair result, we distribute the results of the experiment to 100 people and let them rate them according to their visual experience (five points). We then calculate the average value

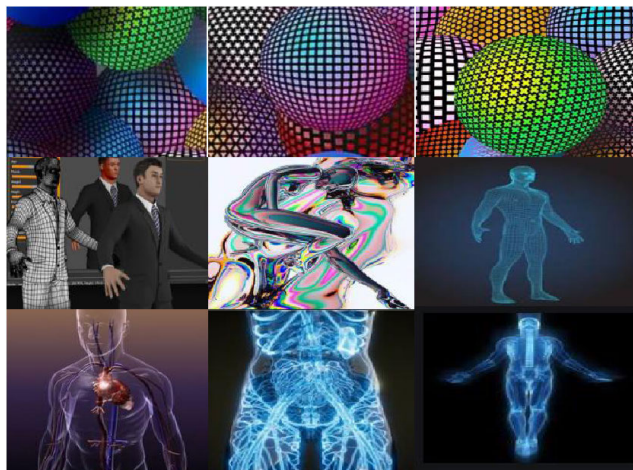


FIGURE 7. Comparison of enhancement results of normal brightness images.

of each algorithm (a total of 500 test images) to judge the pros and cons of various algorithms in the subjective analysis. Figure 7 shows the enhancement effect of various algorithms for some images in the image data set. Besides, we selected three groups of images (low illumination, normal brightness, and highlight), and compared the enhancement results of various algorithms. The color images in the experiment used the YCbCr color space and only processed the Y channel data.

As can be seen from Figure 7, both BBHE and BPCLBHE have the problem of over-enhancement. In their results, the hair color of the wolf body is black, and the nose of the wolf is also the same. The enhancement results of ESIHE, DRSHE, and MEMBER are all visually good, but the noise of the wolf in ESIHE and DRSHE is not much different from the original picture, and it does not have an enhancement effect. The color of the hair on the wolf is comparable to that of MEMBHE. The result is relatively darker. In DRSHE, the hair on the belly of the wolf is white, and the feeling of sunset in the original picture lost. Overall, compared to other contrast algorithms, MEMBHE has moderate contrast enhancement and natural visual effects. The enhancement results of BBHE and ESIHE are both excessive, the body of the tank is black, and the ground in BBHE is white and dazzling. However, the enhancement results of BPCLBHE and DRSHE appear to be insufficient, and the contrast improvement is insufficient. Compared with other contrast algorithms, MEMBHE has moderate contrast stretching and the best effect.

Because subjective analysis is related to the personal visual experience, to reflect the experimental results more accurately, we use information entropy, contrast, and NIQE three objective evaluation indicators of images to measure the enhancement effect of various algorithms. Figure 8 shows some test images and the results of various evaluation indicators. There is a total of 730 images in the test set, and the index results of each algorithm are shown in Figure 8.

The data of D represents the theoretical optimal value, that is, the greater the information entropy, the better (except for

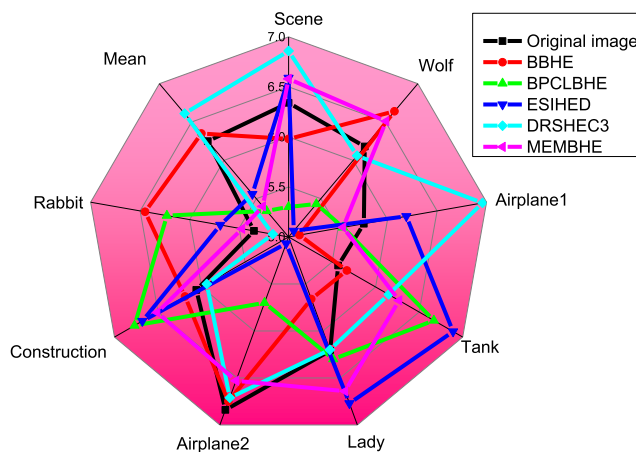


FIGURE 8. Information entropy evaluation index.

the original image, which is only compared in each algorithm), the greater the contrast, the better (which is often not the case in practical applications), and the smaller the NIQE, the better. The greater the information entropy, the fewer gray levels are merged and the more detail is preserved. The greater the contrast, the farther the stretch between the gray levels, the more distinct the layer, but it is also prone to overstretching, so in practical applications, the contrast is often not the greater the better. The smaller the NIQE, the better the visual characteristics of the human eye and the better the visual experience. It can be seen that compared to other comparison algorithms, MEMBHE has the largest information entropy, indicating that it retains the most details; at the same time, it can be seen that the contrast index of BBHE is often the largest, but from the subjective analysis, and it is not prone to excessive enhancement; it can be seen that the NIQE value of MEMBHE is generally small. These results can also be derived from Figure 8. In summary, compared with other comparison algorithms, MEMBHE has moderate contrast improvement, strong detail retention ability, and natural enhancement effect, which is also consistent with the results of our subjective analysis.

The algorithm first uses the Otsu method to obtain the data division points of high-resolution graphics, and divides the high-resolution graphics into two left and right high-resolution graphics; then uses a hybrid pre-processing step to pre-process the high-resolution graphics to enhance the algorithm for the image protection of details; then use the proposed maximum entropy model to perform traversal optimization to obtain the best dynamic range segmentation point, to obtain the corresponding dynamic range when the left and right sub-high resolution graphics are equalized; finally, the left and right sub-high resolution graphics in their corresponding Balanced within the dynamic range of the final enhanced image. Experimental results show that the algorithm proposed in this chapter has moderate contrast improvement, strong detail retention, and good visual effect compared to other contrast algorithms. Since the algorithm uses the traversal optimization method to find the dynamic

range segmentation point, it is suitable for various types of images. The performance is better and the algorithm is robust.

The analysis shows that the optimal cutoff threshold obtained by the hybrid model can make the result image obtain a moderate contrast improvement based on maintaining the image details as much as possible. The change of the index of the mixed model during the traversal of the cutoff threshold is shown in Figure 9.

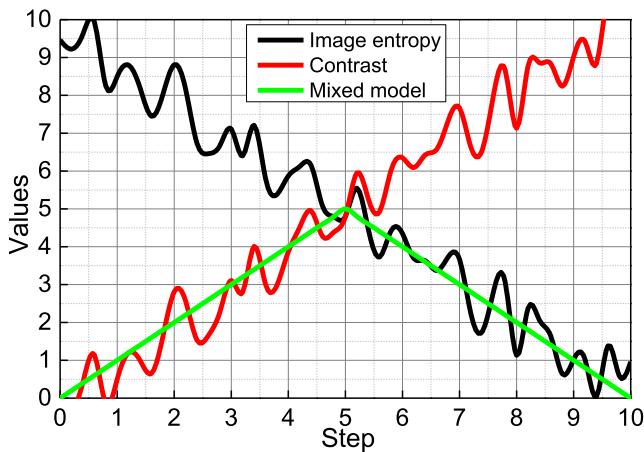


FIGURE 9. Variation curve of mixed model indicators.

As can be seen from Figure 9, as the cutoff threshold increases, the entropy gradually decreases and the contrast gradually increases. In this process, there is an optimal cutoff threshold, that is, the corresponding abscissa in Figure 9, which can make the mixing the model index reaches the maximum, which means that the resulting map retains as much detail as possible while having moderate contrast and the best visual effect. Since the hybrid model adaptively determines the optimal cutoff threshold, it can be applied to various images, and the algorithm is robust.

B. ANALYSIS OF THE EVALUATION RESULTS OF THE IMPLEMENTATION OF AR TECHNOLOGY-AIDED DESIGN SYSTEM

In this article, medium and high dynamic MANET scenarios are selected for simulation testing, in which NDMANET network nodes can move randomly at a certain rate. Suppose that the NDMANET node adopts the IEEE 802.11a protocol at the data link layer, the point-to-point transmission rate is set to 24Mbps, the communication radius of each node is 75m, and the simulation scenario is set to a rectangular area of 600m*600m. The number of nodes is variable, with a range of 60 to 140 and a step value of 20. The moving speed of the node is set to 10m/s (36 km/h), and the node moves randomly. The rate at which consumers send interest packets is 10 per second, and the simulation process lasts 300 seconds. To make the experimental results comparable, the same random number seed and the same random movement model are used when performing simulation experiments on three

different routing algorithms. The above parameter settings for experimental scenarios are summarized in Figure 10.

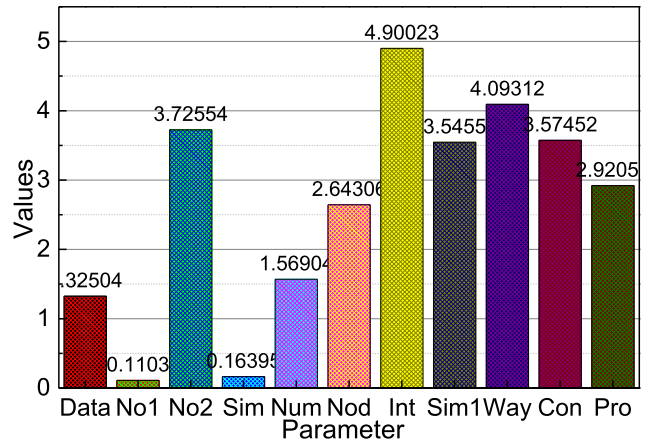


FIGURE 10. Scene parameter settings.

The corresponding curve values of the above three algorithms are positively correlated with the number of nodes. The growth rate of the curve corresponding to the default flooding algorithm is larger, while the growth rate of the curve corresponding to the SPPB and LFBL algorithms is relatively low. The flow increment of the default flooding algorithm increases linearly with the increase of nodes; the flow rate of the LFBL forwarding strategy shows a different rate of increase. The analysis in this article is since the simulation experiment cannot cover all the possibilities to cause different rates of production increase. The traffic of the shortest path backup forwarding strategy is as expected, that is, it is much lower than the flood forwarding strategy. Due to the addition of backup nodes, the traffic is slightly higher than the listening and then broadcast forwarding strategy.

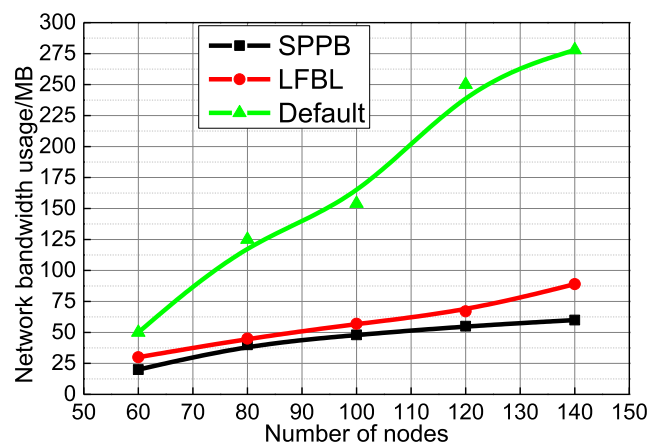


FIGURE 11. Network bandwidth usage.

First, the simulation results of network bandwidth usage are shown in Figure 11, and the experiment counts the total number of packets sent by network nodes. Under all the number of nodes, the default flooding algorithm consumes the largest amount of network bandwidth, and the LFBL

algorithm (shortest path routing algorithm) is the smallest. The SPPB algorithm proposed in this article is only slightly higher than the LFBL algorithm and is still in an Acceptable range. The corresponding curve values of the above three algorithms are positively correlated with the number of nodes.

The growth rate of the curve corresponding to the default flooding algorithm is larger, while the growth rate of the curve corresponding to the SPPB and LFBL algorithms is relatively low. The reason is that the default flood routing algorithm uses broadcast interest packets and broadcast data packets to propagate information packets, while the SPPB and LFBL algorithms can suppress the broadcast of data packets and interest packets. Compared with the LFBL algorithm, the SPPB algorithm constructs a backup path in the NDMANET network. Nodes on this backup path may broadcast interest packets, resulting in the SPPB strategy using slightly higher network bandwidth than the LFBL algorithm.

The simulation result of the average request delay is presented in Figure 11. Overall, the default flooding algorithm produces the highest average request delay, and the SPPB algorithm proposed in this article is the lowest. The LFBL algorithm is slightly higher than the SPPB algorithm, but the difference is not significant. The reason is that in the default flooding method, there are many path relay nodes for the return of some interest packets and data packets, so the time delay is large. In the LFBL algorithm, data packets are returned along the predetermined shortest path, which can greatly reduce the time delay. The SPPB algorithm considers the dynamics of the network topology and provides backup path selection for data packet backhaul, so there is the potential to further reduce the backhaul time. The reason is that the default flood routing algorithm uses broadcast interest packets and broadcast data packets to propagate information packets, while the SPPB and LFBL algorithms can suppress the broadcast of data packets and interest packets. Compared with the LFBL algorithm, the SPPB algorithm constructs a backup path in the NDMANET network. The nodes on this backup path may broadcast interest packets, which causes the SPPB strategy to use network bandwidth slightly higher than the LFBL algorithm.

Overall, the default flooding algorithm generates the highest average request delay, and the SPPB algorithm proposed in this article is the lowest. The LFBL algorithm is slightly higher than the SPPB algorithm. The reason is that in the default flooding method, there are many path relay nodes for the return of some interest packets and data packets, so the time delay is large. In the LFBL algorithm, data packets are returned along the predetermined shortest path, which can greatly reduce the time delay. The SPPB algorithm considers the dynamics of the network topology and provides backup path selection for data packet backhaul, so there is the potential to further reduce the backhaul time. The overall trend of latency is reduced because broadcasting can establish stable communication links as the number of nodes increases.

The experimental result of the request success rate is shown in Figure 12, and the overall situation shows a positive

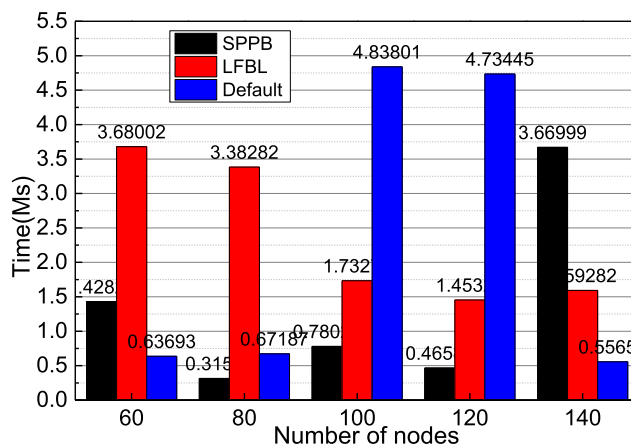


FIGURE 12. Experimental results of average request delay.

correlation with the number of nodes. Since the communication range of network nodes is fixed, in the case of a small number of nodes and a low density, the number of relay nodes is small, so the success rate of data requests is low. As the density of nodes increases, the number of nodes with data relay capabilities gradually increases, and the success rate of requests increases accordingly. The default flooding algorithm uses the broadcast method to send packets, so it can bring the highest request success rate at the cost of maximum network bandwidth usage. The SPPB algorithm proposed in this article has a higher request success rate than the LFBL algorithm. The reason is that the SPPB strategy constructs the shortest path backup path in the network, which reduces the probability of packet return failure so that the request success rate gets a certain degree promote.

Due to the influence of factors such as the random movement model and the number of simulation experiments in the simulation experiment scene, the simulation results show uneven display and different curvature results in the network bandwidth usage, average request delay, and request success rate curves. According to the primary estimate of this paper, in the simulation experiment scenario, when the number of nodes is less than 60, the nodes are too sparse and most of the nodes cannot be networked. When most nodes of the mobile ad hoc network cannot be networked, it is meaningless to study this model of the mobile ad hoc network, so the simulation experiment does not include the experimental data with the number of nodes less than 60.

C. ANALYSIS OF GRAPHIC DESIGN RESULTS

Through the regular arrangement of the shape size and position distribution of the points in the plane space, we can make the plane two-dimensional space produce a three-dimensional visual effect. As shown in the figure below, as shown in Figure 13, the dot structure can make the two-dimensional plane form produce the visual effect of convex and concave in space. In Figure 13, we can also feel the three-dimensional effect produced by the three-dimensional space by arranging

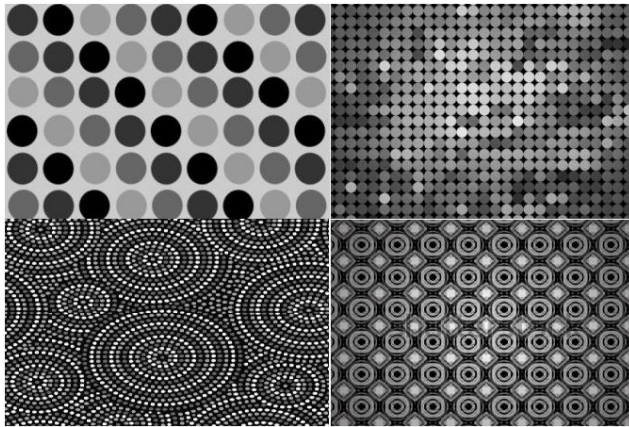


FIGURE 13. The ordered arrangement of points can also form different black, white, and gray levels through the dense and dense relationship, and can also express the undulations of the morphological surface, and even create a three-dimensional space.

the distribution of the points of the negative form at the boundary between the straight line and the straight line.

The ordered arrangement of points in Figure 13 can also form different black, white, and gray levels through the dense and tense relationship. It can also express the undulations of the morphological surface, and even create a three-dimensional space.

The continuous extension of points and points forms a line, which is an important element of the form. By arranging the form of the line, the form can produce different visual effects to form a variety of three-dimensional spatial effects, such as parallel lines changing direction in the middle. There will be a feeling of bumps or waves. By changing the spacing of parallel lines, we will get another sense of visual impact brought about by the line group: the flat space will produce a sense of bulge and depression forward and backward, and more than one line of uneven thickness appears in the picture, the spacing, thickness, and arrangement relationship between them will form different spatial feelings in space, which is related to our perceptual experience. Our understanding of perspective experience is that the front is larger and the smaller, the front is thicker and thinner, the front objects are loosely spaced, and the back appears dense, and the composition of the lines is caused by using this part of human perception experience in vision. The line is a structural representation that can produce a spatial effect, regardless of the thickness, length, light and dark, the dense line group appears to recede than the loose one; the thick line is strong, the thin line is sharp, and the thickness of the line can also produce a distance relationship, the thick line advances, the thin line backward, the solid line advances, and the dashed line backward, which can constitute a three-dimensional structure in the screen.

As shown in Figure 14, the subtle changes in the density and density of line groups bring countless possibilities to three-dimensional space. The three-dimensional vision can also be created by the interweaving of the horizontal and vertical groups of lines, and the regular pattern can be created

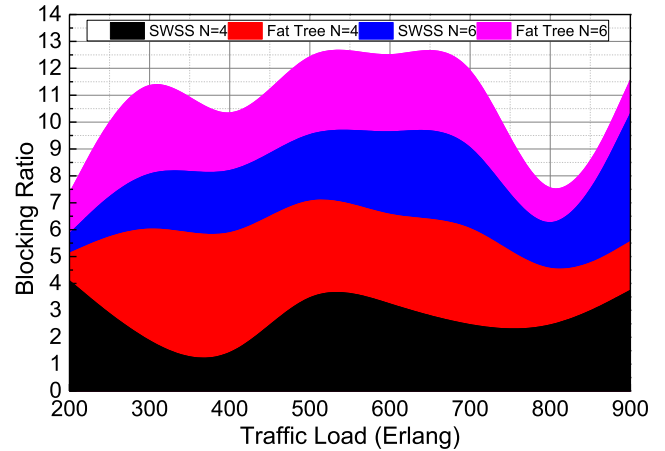


FIGURE 14. Create 3D vision by line.

using bending, thickening, stretching, etc. So that the plane checkerboard pattern can produce a variety of richness.

The line group concentrated to the center can not only cause the dense and dense relationship in the picture, but this morphological change conforms to the law of perspective method, has a strong suggestive effect, can form a strong sense of distance, and expand the depth of the plane three-dimensional space.

This section compares and evaluates the performance of the SWSS and fat-tree in three aspects of blocking rate, bandwidth utilization, and normalized hop count under non-random traffic. This section defines the traffic localization factor (Traffic Locator, TLF) to measure non-random traffic, which refers to the ratio of the internal and external traffic of the cluster. For example, in SWSS, as shown in Figure 15.

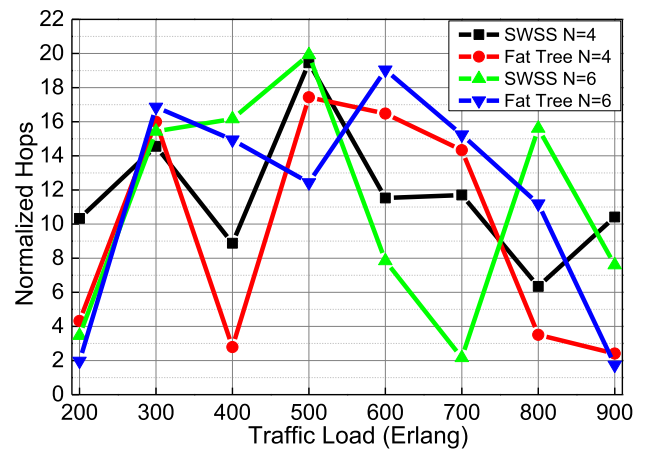


FIGURE 15. Comparison of graphic design hops under different random traffic loads.

For the algorithms after the motion recovery structure, these algorithms are mainly some algorithms in computer graphics. If the motion recovery structure provides rough spatial information, the geometric processing algorithm extracts fine three-dimensional geometric information. It is

not enough to have a motion recovery structure. It can be said that it is halfway. Only if the grid is extracted from the point cloud is it truly a 3D reconstruction. The use of geometric processing algorithms often depends on the different needs in the actual scene. After surface reconstruction, it can be seen from the experimental results that the 3D model has greatly improved its quality, which also provides a guarantee for more post-processing.

V. CONCLUSION

This article studies graphic design through an improved high-resolution graphics processing algorithm, and uses a real-time AR technology system to conduct in-depth discussions, introduces the theoretical basis of high-resolution graphics equalization and some image quality evaluation indicators, and divides the current improved algorithms into two categories: brightness maintenance and variable brightness. The algorithm uses the maximum entropy model to find the best dynamic range segmentation point to achieve a certain degree of adaptability. The preprocessing process strengthens the algorithm's ability to maintain details. Experiments show that this algorithm has a wider application range than brightness-maintaining algorithms, and it has better details retention ability than other brightness-variable algorithms. The maximum entropy model is improved to solve the problem of its failure due to the constant image entropy during the equalization process. A global high-resolution graphic equalization based on a hybrid model and a post-processing scheme for high-resolution graphics are proposed. It uses a hybrid model to determine the optimal cutoff threshold for high-resolution graphics; post-processing further enhances the ability to maintain detail. Experiments show that the algorithm has a wide application range, strong detail retention ability, natural processing effect, and low computational complexity. It can be used for real-time video enhancement and graphic design and has strong practicability.

REFERENCES

- [1] C.-T. Cheng, T.-Y. Ho, T.-Y. Lee, C.-C. Chang, C.-C. Chou, C.-C. Chen, I.-F. Chung, and C.-H. Liao, "Application of a deep learning algorithm for detection and visualization of hip fractures on plain pelvic radiographs," *Eur. Radiol.*, vol. 29, no. 10, pp. 5469–5477, Feb. 2019.
- [2] H.-Z. Hu, X.-B. Feng, Z.-W. Shao, M. Xie, S. Xu, X.-H. Wu, and Z.-W. Ye, "Application and prospect of mixed reality technology in medical field," *Current Med. Sci.*, vol. 39, no. 1, pp. 1–6, Feb. 2019.
- [3] S. Sylaiou, K. Mania, I. Paliokas, L. Pujol-Tost, V. Killintzis, and F. Liarakis, "Exploring the educational impact of diverse technologies in online virtual museums," *Int. J. Arts Technol.*, vol. 10, no. 1, pp. 58–84, Apr. 2017.
- [4] G. Priestnall, E. FitzGerald, S. Meek, M. Sharples, and G. Polmear, "Augmenting the landscape scene: Students as participatory evaluators of mobile geospatial technologies," *J. Geography Higher Educ.*, vol. 43, no. 2, pp. 131–154, Apr. 2019.
- [5] I. Pachoulakis, D. Tsilidi, and A. Analyti, "Computer-aided rehabilitation for the carpal tunnel syndrome using exergames," *Adv. Image Video Process.*, vol. 6, no. 2, p. 44, Apr. 2018.
- [6] M. A. Martens, A. Antley, D. Freeman, M. Slater, P. J. Harrison, and E. M. Tunbridge, "It feels real: Physiological responses to a stressful virtual reality environment and its impact on working memory," *J. Psychopharmacol.*, vol. 33, no. 10, pp. 1264–1273, Oct. 2019.
- [7] H.-Z. Hu, X.-B. Feng, Z.-W. Shao, M. Xie, S. Xu, X.-H. Wu, and Z.-W. Ye, "Application and prospect of mixed reality technology in medical field," *Current Med. Sci.*, vol. 39, no. 1, pp. 1–6, Feb. 2019.
- [8] Z. Al-Kassim and Q. A. Memon, "Designing a low-cost eyeball tracking keyboard for paralyzed people," *Comput. Electr. Eng.*, vol. 58, pp. 20–29, Feb. 2017.
- [9] S. Colantonio, G. Coppini, D. Giorgi, M.-A. Morales, and M. A. Pascali, "Computer vision for ambient assisted living: Monitoring systems for personalized healthcare and wellness that are robust in the real world and accepted by users, carers, and society," in *Proc. Comput. Vis. Assistive Healthcare*, Jan. 2018, pp. 147–182.
- [10] A. Seba, N. Nouali-Taboudjemat, N. Badache, and H. Seba, "A review on security challenges of wireless communications in disaster emergency response and crisis management situations," *J. Netw. Comput. Appl.*, vol. 126, pp. 61–150, Jan. 2019.
- [11] C. Fang, P. Zhang, and X. Qi, "Digital and intelligent liver surgery in the new era: Prospects and dilemmas," *EBioMedicine*, vol. 41, pp. 693–701, Mar. 2019.
- [12] R. Alarcon, F. Wild, C. Perey, M. M. Genescà, J. G. Martínez, J. X. Ruiz Martí, M. J. Simon Olmos, and D. Dubert, "Augmented reality for the enhancement of space product assurance and safety," *Acta Astronaut.*, vol. 168, pp. 191–199, Mar. 2020.
- [13] P.-U. Malmström, S. Agrawal, M. Bläckberg, P. J. Boström, B. Malavaud, D. Zaak, and G. G. Hermann, "Non-muscle-invasive bladder cancer: A vision for the future," *Scandin. J. Urol.*, vol. 51, no. 2, pp. 87–94, Mar. 2017.
- [14] E. I. Liem and T. M. de Reijke, "Can we improve transurethral resection of the bladder tumour for nonmuscle invasive bladder cancer?" *Current Opinion Urol.*, vol. 27, no. 2, pp. 149–155, Mar. 2017.
- [15] I. Ishafit, T. K. Indratno, and Y. D. Prabowo, "Arduino and LabVIEW-based remote data acquisition system for magnetic field of coils experiments," *Phys. Educ.*, vol. 55, no. 2, Dec. 2019, Art. no. 025003.
- [16] H. Wang, E. Sun, F. Feifei, and S. Liu, "A framework of a 3D DCPCS based on UWB positioning in underground mining," *Int. J. Georesources Environ.*, vol. 4, no. 3, pp. 153–162, Jul. 2018.
- [17] P. Pouladzadeh, P. Kuhad, S. V. B. Peddi, A. Yassine, and S. Shirmohammadi, "Food calorie measurement using deep learning neural network," in *Proc. IEEE Int. Instrum. Meas. Technol. Conf.*, May 2016, pp. 1–6.
- [18] S. Ding, L. Feng, J. Wu, F. Zhu, Z. Tan, and R. Yao, "Bioprinting of stem cells: Interplay of bioprinting process, bioinks, and stem cell properties," *ACS Biomater. Sci. Eng.*, vol. 4, no. 9, pp. 3108–3124, Jul. 2018.
- [19] S. Balasubramanian, J. Chenniah, G. Balasubramanian, and V. Vellaipandi, "The era of robotics: Dexterity for surgery and medical care: Narrative review," *Int. Surg. J.*, vol. 7, no. 4, pp. 1317–1323, Mar. 2020.
- [20] P. Ji, S.-U. Baek, C.-H. Park, S.-S. Lee, Y.-E. Im, and Y. Choi, "Inline fiber optic power sensor featuring a variable tap ratio based on a tightly focused femtosecond laser inscription," *Opt. Express*, vol. 26, no. 12, pp. 14972–14981, Jun. 2018.
- [21] F. Chen, Q. Wu, D. Song, X. Wang, P. Ma, and Y. Sun, "Fe₃O₄@PDA immune probe-based signal amplification in surface plasmon resonance (SPR) biosensing of human cardiac troponin I," *Colloids Surf. B, Biointerfaces*, vol. 177, pp. 105–111, May 2019.
- [22] A. M. Doshi, W. H. Moore, D. C. Kim, A. B. Rosenkrantz, N. R. Fefferman, D. L. Ostrow, and M. P. Recht, "Informatics solutions for driving an effective and efficient radiology practice," *Radiographics*, vol. 38, no. 6, pp. 1810–1822, Oct. 2018.
- [23] E. I. Konstantinidis, G. Bamparopoulos, and P. D. Bamidis, "Moving real exergaming engines on the Web: The WebFitForAll case study in an active and healthy ageing living lab environment," *IEEE J. Biomed. Health Informat.*, vol. 21, no. 3, pp. 66–859, Apr. 2016.
- [24] A. Lapico, M. Sankupellay, L. Cianciullo, T. Myers, D. A. Kononov, D. R. Jerry, P. Toole, D. B. Jones, and K. R. Zenger, "Using image processing to automatically measure pearl oyster size for selective breeding," in *Proc. Digit. Image Comput., Techn. Appl. (DICTA)*, Dec. 2019, pp. 1–8.
- [25] S. Pearce and S. Daneshmand, "Enhanced endoscopy in bladder cancer," *Current Urol. Rep.*, vol. 19, no. 10, p. 84, Oct. 2018.
- [26] T.-Y. Tai, H. H.-J. Chen, and G. Todd, "The impact of a virtual reality app on adolescent EFL learners' vocabulary learning," in *Proc. Comput. Assist. Lang. Learn.*, Apr. 2020, pp. 1–26.
- [27] A. Tou, H.-H. Kim, H. Einaga, Y. Teramoto, and A. Ogata, "Ozone-assisted catalysis of CO: *In situ* Fourier transform IR evidence of the cooperative effect of a bimetallic Ag-Pd catalyst," *Chem. Eng. J.*, vol. 355, pp. 380–389, Jan. 2019.

- [28] T. Rikakis, A. Kelliher, J. Choi, J.-B. Huang, K. Kitani, S. Zilevu, and S. L. Wolf, "Semi-automated home-based therapy for the upper extremity of stroke survivors," in *Proc. 11th Pervas. Technol. Rel. Assistive Environ. Conf.*, Jun. 2018, pp. 249–256.
- [29] R. Hu, T. Fan, J. Yang, H. Xiao, Y. Liu, and M. Lu, "Ultrasound and microwave technology for flake-TiO₂ growth and immobilization on cotton fabrics in micro-dissolution process," *Mater. Chem. Phys.*, vol. 249, Jul. 2020, Art. no. 123036.
- [30] P. Rahi, S. P. Sood, and R. Bajaj, "Smart platforms of air quality monitoring: A logical literature exploration," in *Proc. Int. Conf. Futuristic Trends Netw. Comput. Technol.*, Nov. 2019, pp. 52–63.
- [31] A. Keshavarzi and W. van den Hoek, "Edge intelligence—On the challenging road to a trillion smart connected IoT devices," *IEEE Des. Test.*, vol. 36, no. 2, pp. 41–64, Apr. 2019.
- [32] S. Céspedes, J. Salamanca, A. Yáñez, and D. Vinasco, "Group cycling meets technology: A cooperative cycling cyber-physical system," *IEEE Trans. Intell. Transp. Syst.*, vol. 20, no. 8, pp. 3178–3188, Aug. 2019.
- [33] M. Chen, S. Lu, and Q. Liu, "Uniform regularity for a Keller–Segel–Navier–Stokes system," *Appl. Math. Lett.*, vol. 107, Sep. 2020, Art. no. 106476.
- [34] M. Manikandan, A. Deenadayalan, A. Vimala, J. Gopal, and S. Chun, "Clinical MALDI mass spectrometry for tuberculosis diagnostics: Speculating the methodological blueprint and contemplating the obligation to improvise," *TrAC Trends Anal. Chem.*, vol. 94, pp. 190–199, Sep. 2017.



TING SHENG was born in Wuhan, Hubei, China, in 1980. She received the bachelor's and master's degrees from the Hubei Institute of Fine Arts, in 2002 and 2006, respectively. She is currently working at the Wuchang University of Technology. She has published five core articles. Her research interest includes graphic design.

• • •